

---

# Thermal processing of hydroxyapatite for coating production

---

K. A. Gross, C. C. Berndt

Thermal Spray Laboratory, Department of Materials Science and Engineering, State University of New York at Stony Brook, New York 11794-2275

Received 17 January 1997; accepted 12 March 1997

**Abstract:** Thermally processed hydroxyapatite coatings used on dental implants and hip prostheses for enhanced fixation may typically consist of a number of chemical and structural phases. These phases affect coating performance and tissue attachment. Hydroxyapatite was plasma sprayed to examine the phase evolution during processing. Coatings were examined with X-ray diffraction and elemental analysis. Results indicate that phase transformations are produced by (a) preferential removal of hydroxyl and phosphate leading to a change in melt composition, and (b) the high cooling rate due to the thermal spray process. Hydroxyl group removal promotes the amorphous phase and oxyapatite. Further heating produces a less viscous melt fa-

cilitating decomposition of hydroxyapatite to tricalcium and tetracalcium phosphate. Phosphate removal during flight produces a more calcium-rich melt preferring tetracalcium phosphate and calcium oxide formation. A proposed model shows the phase location within the lamellae of these coatings. Coating processes must thus prevent removal of hydroxide and phosphate during processing to maximize the hydroxyapatite content. © 1998 John Wiley & Sons, Inc. *J Biomed Mater Res*, 39, 580-587, 1998.

**Key words:** plasma spraying; hydroxyapatite; decomposition; vaporization; amorphous; X-ray diffraction

---

## INTRODUCTION

Hydroxyapatite has been recognized for its biocompatibility and usefulness in promoting biointegration for implants in osseous and soft tissue. The range of applications cover diversity such as microbial seals in middle-ear implants, orbital implants for artificial eyes,<sup>1</sup> percutaneous devices for drug delivery,<sup>2</sup> augmentation in maxillofacial surgery<sup>3</sup> or increasing bone depth in mandibles: coatings on cylindrical posts for dental implants,<sup>5</sup> and artificial ears and coated stems for hip prostheses.<sup>6</sup> The wide application in the body signifies its importance as a biomaterial.

The function of implants is dependent upon the manufacture route chosen for fabrication. Most techniques used in industry for the preparation of hydroxyapatite employ a heat source for consolidation of powder to a sintered monolith or a coating. Coating technologies which have been used in the laboratory setting include pulsed laser deposition,<sup>7</sup> magnetron sputtering,<sup>8</sup> and thermal spraying. Plasma spraying is

widely used for manufacturing hydroxyapatite coatings on titanium or Co-Cr-based alloy implants in industry. The main emphasis in this report is placed on thermal spraying with reference to the other methods.

Preparation of hydroxyapatite coatings is confronted with a multitude of phase changes that occur at high temperatures. Material injected into a plasma may be heated to several thousand degrees centigrade and propelled at high speeds to the substrate to form a coating. These extreme heating and cooling conditions can produce metastable phases as a result of rapid cooling from a high temperature. Hydroxyapatite coatings can be accompanied with oxyapatite, tetracalcium phosphate, tricalcium phosphate, calcium oxide, and the amorphous phase. The complexity of coating manufacture results from the rich thermal chemistry and, therefore, technological progress is often delayed since manufacturing methods are commercial secrets.

The solubility and ability to bond to osseous tissue depends on the crystal phase. Tetracalcium phosphate dissolves quickly<sup>9</sup> and calcium oxide reacts rapidly in aqueous environments. Dissolution increases in the order of hydroxyapatite, tetracalcium phosphate, tricalcium phosphate, and the amorphous phase.<sup>10</sup> A stable coating can be produced by minimizing the more soluble phases so that biointegration can become

Correspondence to: K. A. Gross, Department of Materials Engineering, Monash University, Clayton, Victoria 3168, Australia

established on the hydroxyapatite. The reliable manufacture of hydroxyapatite requires good process control to be able to predict *in vivo* coating performance. This article discusses the phase transformations that can be formed from plasma spraying hydroxyapatite based on the phases that have been determined by X-ray diffraction.

**Equilibrium phase diagram including hydroxyapatite**

The phase composition of the coating formed by plasma spraying depends on the thermal history of the

hydroxyapatite powder as it passes through the flame. An equilibrium phase diagram'' can be used as a first step in predicting the phases that could form upon solidification. The region of interest shaded in Figure 1(b) is bounded by two stoichiometric compounds: tetracalcium phosphate (with a chemical formula of  $Ca_4P_2O_9$ , designated as "C<sub>4</sub>P") and tricalcium phosphate [with a chemical formula of  $Ca_3(PO_4)_2$ , designated as "C<sub>3</sub>P"]. At zero partial water pressure, hydroxyapatite [ $Ca_{10}(PO_4)_6(OH)_2$ ] is not expected to form [Fig. 1(a)]. A combination of tetracalcium phosphate and tricalcium phosphate will exist at high temperatures and will remain at a constant phase compo-

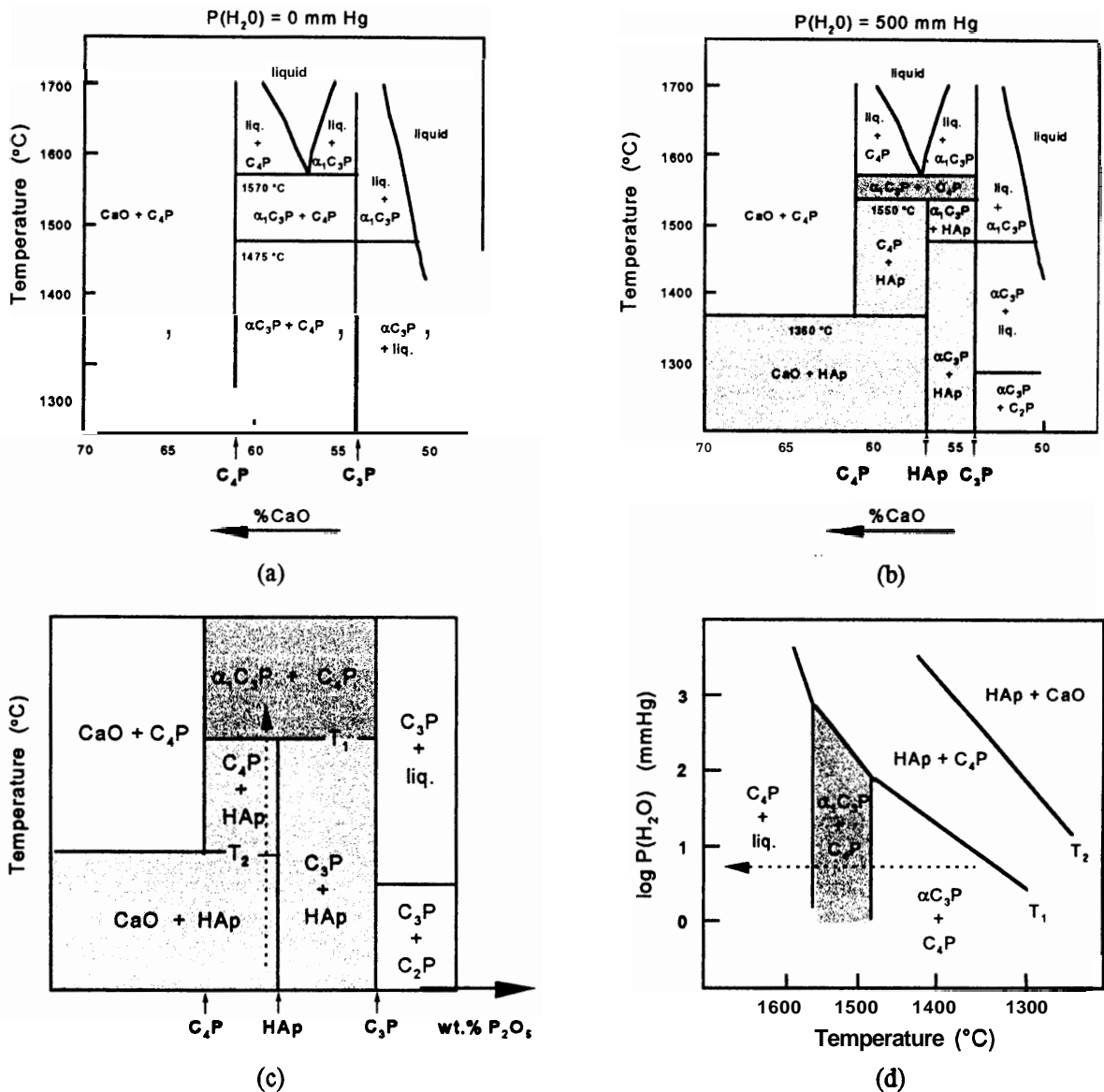


**Figure 1.** Phase diagram illustrating the (a) phases at 0 mm Hg, (b) phases at 500 mm Hg, (c) simplified illustration of the high-temperature region, and (d) effect of partial water pressure on the stability field of the calcium phosphate phases. The light gray regions in (b) and (c) refer to the additional phases surrounding the hydroxyapatite phase. The dark gray region in (b) and (c) represents the two phase, C<sub>3</sub>P and C<sub>4</sub>P region, and the shaded region indicated in (d) shows the phase dependence of C<sub>3</sub>P and C<sub>4</sub>P on the partial water vapor pressure.

sition down to low temperatures. Only the structure of tricalcium phosphate will change upon cooling. The high temperature polymorph of tricalcium phosphate ( $\alpha_1$ - $C_3P$ ) will not form on quenching<sup>12</sup> but will change to  $\beta$ -TCP under slow cooling conditions or a metastable  $\alpha$ -type of  $C_3P$ <sup>13</sup> when subject to faster cooling.

If the partial water pressure is sufficiently high, hydroxyapatite is introduced as a stable stoichiometric compound with a composition of 55 wt % CaO. The number of phase regions around the hydroxyapatite composition increase and are indicated with light gray shading. At a partial water vapor pressure of 500 mm Hg, hydroxyapatite is stable up to about 20°C below the melting temperature [Fig. 1(b)]. The temperature range of the two-phase region increases to a maximum range of 75°C when the partial water pressure decreases to 100 mm Hg.

The thermal chemistry is complex at submelting temperatures; thus, the relevant area indicated by dark gray shading is expanded for clarity [Fig. 1(c)]. If a calcium phosphate is heated to follow the arrow in Figure 1(c), the two-phase region would be encountered before eutectic melting. This is also shown in Figure 1(d) to indicate the effect of the water vapor pressure. Increasing water vapor pressure will decrease the temperature range of the two-phase region. Heating of hydroxyapatite with a water vapor pressure higher than 900 mm Hg avoids decomposition, and melting occurs.

## MATERIALS AND METHODS

### Coating preparation

A Metro 3MB plasma spray torch with a GH nozzle was used to spray 5-40  $\mu\text{m}$  spherical hydroxyapatite powder. Powder was injected external to the gun and perpendicular to the plasma flow. The torch was operated at different power levels with argon as the primary plasma gas and nitrogen added to increase the plasma enthalpy. Where the power level is not indicated, the argon flow was changed with the torch at 18 kW. This allowed determination of the processing condition influence on the phase content of the coatings. Prior to spraying, substrates were grit blasted with 40-mesh SiC powder.

The feedstock powder was characterized by thermal analysis and X-ray diffraction. Differential thermal analysis (DTA) was performed along with the thermal gravimetric analysis (TGA). This enabled changes in weight of the 20-mg sample to be correlated with reactions observed in the DTA trace. The powder sample was heated at 5°C/min to 1400°C in static air. The variability in the signal was 0.25 wt % for TGA and approximately  $5.7 \times 10^{-3} \mu\text{V/g}$  for DTA. X-ray diffraction examination was carried out with Cu  $K\alpha_1$  radiation of  $\lambda = 1.54 \text{ \AA}$ . The goniometer was set at a scan rate of 0.01°/s over a  $2\theta$  range of 20°–60°.

The extent of hydroxyapatite decomposition was examined by determining the Ca/P ratio of the coatings after removal from the substrate. Table I illustrates the Ca/P molar ratio for the decomposition of known crystalline calcium phosphate phases. The calcium and phosphorus concentrations were determined with X-ray fluorescence and compared to the hydroxyapatite powder used for spraying. Decomposition phases were ascertained using X-ray diffraction on the as-sprayed coating surface.

A coating was sectioned and the cross section mounted in an epoxy resin. It was then polished to reveal the phase structure of the coating. Observation of the microstructure was performed with a light microscope.

## RESULTS AND DISCUSSION

### Phase formation in thermal spraying

Rapid heating of hydroxyapatite particles to a molten condition and subsequent deposition in plasma spraying mainly produces hydroxyapatite (Fig. 2). This implies that the cooling rate is sufficiently high to suppress short-range diffusion necessary for tricalcium phosphate and tetracalcium phosphate formation, as can be expected from the two-phase region beneath the eutectic point. Undercooling of approximately 0.2 of the melting temperature ( $T_m$ ) can also take place during the higher cooling rates in splat cooling.<sup>14</sup> The solidification temperature of a melt with the composition of hydroxyapatite with such an undercooling would be lowered from 1570°C to 1200°C, which is sufficient to lower the solidification temperature beneath the two-phase region,  $C_3P$  and  $C_4P$ , allowing hydroxyapatite to form. The lack of dif-

TABLE I  
Calcium-Containing Compounds in Calcium Phosphate System

Calcium phosphate	Chemical Formula	Ca/P Ratio	JCPDS No.
Calcium pyrophosphate	$\text{Ca}_2\text{P}_2\text{O}_7$	$2\text{CaO} \cdot \text{P}_2\text{O}_5$	1 2-647
Tricalcium phosphate	$\alpha\text{-Ca}_3(\text{PO}_4)_2$	$3\text{CaO} \cdot \text{P}_2\text{O}_5$	1.5 9-348
Hydroxyapatite	$\text{Ca}_{10}(\text{PO}_4)_6(\text{OH})_2$	$10\text{CaO} \cdot 3\text{P}_2\text{O}_5 \cdot \text{H}_2\text{O}$	1.67 9-432
Oxyapatite	$\text{Ca}_{10}(\text{PO}_4)_6\text{O}$	$10\text{CaO} \cdot 3\text{P}_2\text{O}_5$	1.67
Tetracalcium phosphate	$\text{Ca}_4\text{P}_2\text{O}_9$	$4\text{CaO} \cdot \text{P}_2\text{O}_5$	2 25-1137
Calcium oxide	CaO	CaO	- 4-777

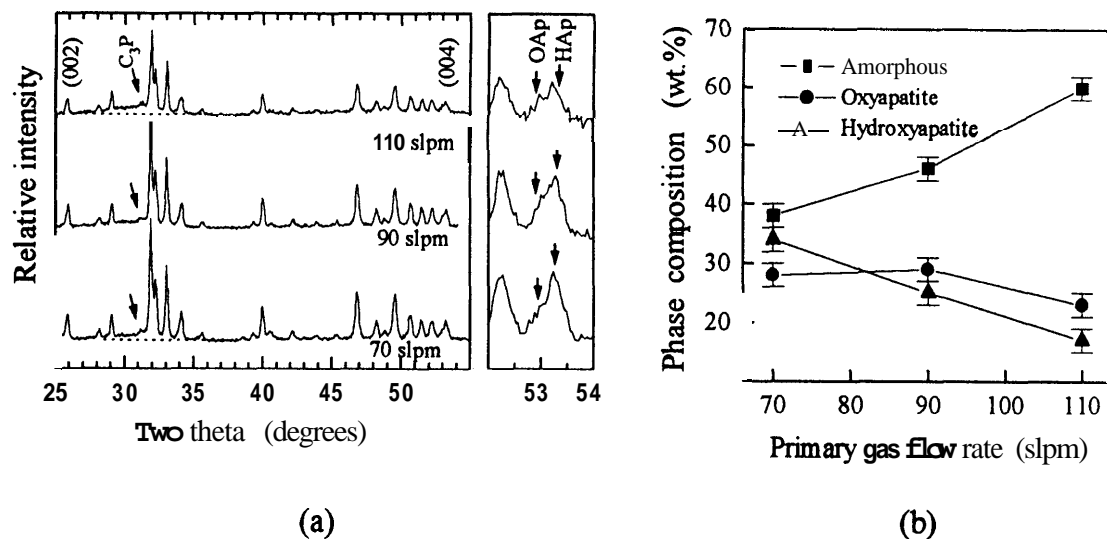


Figure 2. X-ray diffraction spectra of hydroxyapatite coatings produced at (a) increasing plasma gas flow rate. The amount of the amorphous phase, hydroxyapatite, and oxyapatite is shown in (b).

fusion and the undercooling in the rapidly cooled particles thus encourage hydroxyapatite to form.

An amorphous phase is also detected in hydroxyapatite coatings (Fig. 2). This is identified as a broad hump in the X-ray diffraction spectra (produced with CuK $\alpha$  radiation) centered at about 31° and slightly elevated from the background [Fig. 2(a), bottom pattern]. The amount of amorphous phase formed is dependent upon the cooling rate,<sup>15</sup> which may be modified according to the substrate or coating temperature.<sup>16</sup> A more fluid particle will spread to a greater degree to produce higher heat withdrawal rates from the impacted droplet (i.e., higher cooling rate) preventing crystallization of the complex structure of hydroxyapatite.

The hydroxide content of the molten particle before impact is also important. Hydroxyapatite feedstock powder may be hydroxyl deficient initially or may undergo removal from heating in the plasma. Thermal analysis of the feedstock powder used in this experiment (Fig. 3) illustrates a slow exothermic response weight gain up to about 1000°C arising from moisture uptake into the lattice. Further heating above this temperature produces dehydroxylation which requires an input of energy, and hence, endothermic behavior in the DTA curve coupled with a weight loss in the TGA curve. In a thermal source such as a plasma, the fast heating and high temperatures attained in this process will cause hydroxyl removal. The lower driving force for crystallization of the hydroxyl-depleted regions in the molten droplet further promotes amorphous phase formation. Avoiding the amorphous phase formation is difficult and is possible only by ensuring low hydroxyl loss or a sufficiently high substrate temperature. The temperature for crystallization of hydroxyl depleted regions is higher than regions of stoi-

chiometric hydroxyapatite and requires a temperature of 700°C.

Some hydroxyl-deficient regions which do not form the amorphous phase will undergo crystallization to oxyapatite. This can be identified in an X-ray diffraction pattern. The c-axis of the unit cell of oxyapatite is slightly larger than hydroxyapatite, producing peak splitting on those planes with a component in the c-axis direction. The small crystal size and the large defect concentration from the fast cooling produce a broadening in the peaks making phase detection difficult. Focusing on the (004) peak at the large-angle regime of the X-ray diffraction pattern where peak separation is more evident, a shoulder is observed on the left side of the peak at 53.1° [Fig. 2(a)]. The coating was produced without a secondary gas to remove the contribution of added enthalpy. Increase in plasma gas flow rate transports the droplet at a higher speed,

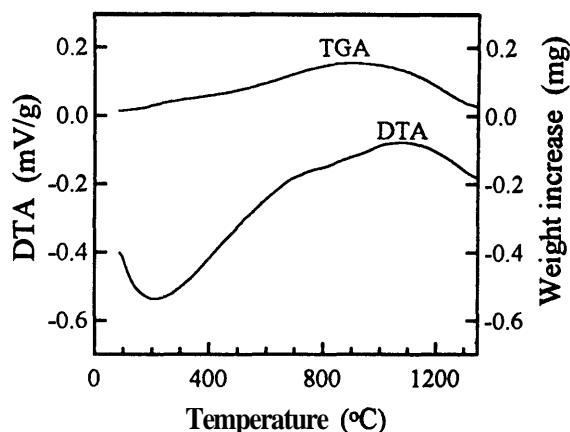


Figure 3. Analysis of hydroxyapatite powder with thermal gravimetric analysis and differential thermal analysis in an alumina crucible and static air.

and so more of the hydroxyl depleted regions are consumed in the amorphous phase as opposed to forming oxyapatite. This interplay of oxyapatite and amorphous content [Fig. 2(b)] is solely dependent upon the cooling rate. Hydroxyapatite is less sensitive to the cooling rate.

A small amount of tricalcium phosphate is often associated with crystalline hydroxyapatite [Fig. 2(a)]. This can be explained with reference to the equilibrium phase diagram [Fig. 1(b)]. Hydroxyapatite has a hypereutectic composition, slightly phosphate rich compared to the eutectic point ( $-57$  wt % CaO). The phases at melting under equilibrium conditions thus consist of tricalcium phosphate and a liquid with eutectic composition. Cooling produces primary tricalcium phosphate until the remaining liquid solidifies. The small amount of tricalcium phosphate accompanying hydroxyapatite is a characteristic of the material system and has been incorporated into the standards controlling the coating quality.<sup>17</sup>

#### Phases produced by decomposition and vaporization

As the power level of the torch increased to supply more heat to the injected particles, the CaO phase appeared. This is not obvious from the phases predicted in the equilibrium diagram.

The rise in the Ca/P molar ratio of coatings produced at increasing power levels (Table II) signified a change in chemistry during spraying which could be related to additional phases. Vaporization of powders injected into the plasma<sup>18</sup> can produce preferential removal. For example, carbon removal from tungsten carbides<sup>19,20</sup> and copper removal from  $\text{YBa}_2\text{Cu}_3\text{O}_{7-\delta}$  superconductors<sup>21</sup> has been reported in thermal sprayed coatings. Heating of calcium phosphates for study of phases<sup>22</sup> or during rf-sputtering<sup>23</sup> preferentially removes the phosphate group. Plasma spraying of hydroxyapatite also preferentially removes the lower melting point component, with the amount depending upon the heat transfer. The change in chemistry occurs on the outside of the molten particle where the heating conditions are the most intense and phosphate removal is easiest. A 4.4 wt % change in the phosphate content is sufficient to provide a composi-

TABLE II  
Influence of Power Level on Decomposition of Hydroxyapatite to Crystalline Phases

Power level (kW)	18	24	30	36
Ca/P molar ratio	1.67	1.69	1.75	2.03
Phases	HAp, C <sub>3</sub> P	HAp, C <sub>3</sub> P	HAp, C <sub>3</sub> P, C <sub>4</sub> P	HAp, C <sub>3</sub> P, C <sub>4</sub> P, CaO

tion shift into the adjacent phase field [Fig. 1(b)] necessary for the formation of calcium oxide (CaO) and C<sub>4</sub>P. The amount of these phases depends upon the extent of heat transfer and is dictated by the particle size, particle velocity, and location within the flame of traversing particles.

Wang et al.<sup>24</sup> reported an increase in Ca/P ratio of plasma-sprayed coatings by employing different secondary gases, but found a smaller increase (from 1.69 to 1.85). This is believed to be due to the larger particle size used in that study. Results of McPherson et al.<sup>25</sup> in which a larger particle size distribution was used for spraying, agree with the present research results.

This study shows tricalcium phosphate coexisting with hydroxyapatite, an amorphous phase and perhaps oxyapatite at low power levels (i.e., 18 kW) (Fig. 4). The presence of tetracalcium phosphate at higher levels (i.e., 24 kW) is not as obvious, owing to a smaller amount on decomposition (Eq. 1), but at higher power levels, the concentration is supplemented by the formation of both C<sub>4</sub>P and CaO. The small particle size and the dehydroxylated state of the powder promoted decomposition. Ellies et al.<sup>26</sup> reported both C<sub>3</sub>P and CaO as decomposition phases, but failure to locate C<sub>4</sub>P could have been due to overlapping with hydroxyapatite peaks. The overlapping of peaks from the various calcium phosphates and CaO is shown in Figure 5. Yang et al.<sup>27</sup> conducted a parameter study and found the influence of power level and stand-off distance on the amount of HAp, C<sub>3</sub>P, C<sub>4</sub>P, and CaO. Knepper<sup>28</sup> also examined the decomposition products

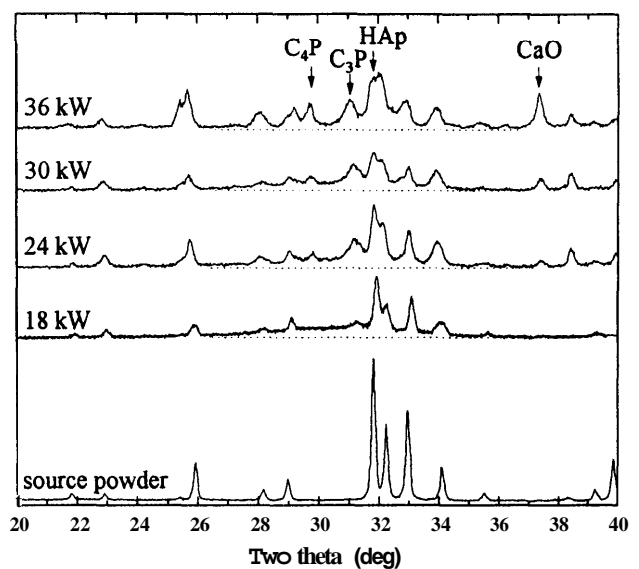


Figure 4. Decomposition phases of hydroxyapatite after plasma spraying at incremental power levels. The main peaks of hydroxyapatite,  $\alpha$ -tricalcium phosphate, tetracalcium phosphate, and calcium oxide are shown. The pattern of the starting powder is given for comparison. The amorphous phase is shown as the rise above the background indicated as a dotted line. Oxyapatite is not indicated.

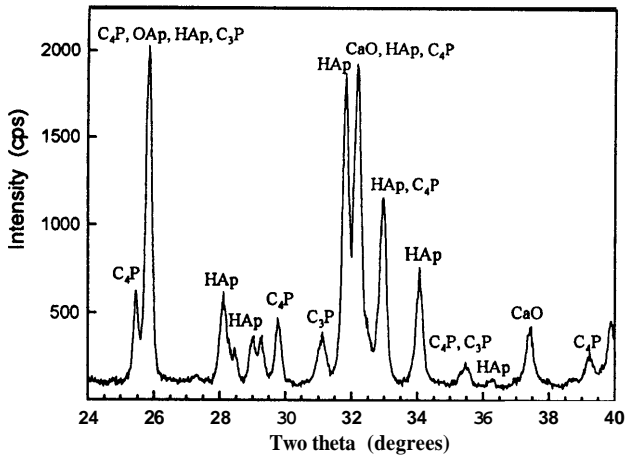
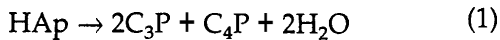


Figure 5. Overlapping of the main crystalline phases within hydroxyapatite coatings. The amorphous phase has been removed by heat treatment.

in vacuum plasma spraying and found a higher decomposition at lower pressures.



**Model for phase formation in hydroxyapatite coatings**

The presence of hydroxyapatite, the amorphous phase, oxyapatite, tricalcium phosphate, tetracalcium phosphate, and calcia has been shown, but the location within the lamellae has not been discussed. A model presented by Khor and Cheang,<sup>29</sup> in which the outside skin of a particle is molten and the core is unmolten, depicts only one possibility in which insufficient heat is transferred to melt the particle completely. This model must be modified to a totally molten hydroxyl-rich core (with the stoichiometry of hydroxyapatite) with further changes depending on the heat transfer to the particle. A more heat-affected particle volume will be indicated as a shell; however, it should be stressed that under intense heating conditions, the changes could also apply to the core of the particle.

The first condition depicts a molten droplet with a hydroxyl-depleted skin. The center containing the hydroxyl-rich molten material will crystallize upon deposition to form hydroxyapatite. The dehydroxylated region, which comes into contact with the substrate upon droplet spreading, will form the amorphous phase, but the area distant from the substrate will crystallize to form oxyapatite. Oxyapatite requires smaller atomic rearrangements to occur for crystallization from a viscous melt, and therefore crystallizes in preference to tricalcium phosphate and tetracalcium phosphate. Growth of the apatite which begins as hydroxyapatite in the hydroxyl-rich core will thus

change to oxyapatite in response to the depleted hydroxyl concentration at the top of the lamellae. This is shown in Figure 6, case (i). If the molten particle flattens to an extent where the cooling rate is increased, then the entire particle becomes amorphous. Primary tricalcium phosphate is not shown.

The proposed model can be extended to incorporate other phases observed at higher heating conditions. Tricalcium phosphate and tetracalcium phosphate are observed in greater quantities when a higher heat transfer to the particle prevails. If the heat dissipation is slow through the already-solidified amorphous and crystalline layers of the coating, tricalcium phosphate and tetracalcium phosphate can be nucleated at the top surface of the lamellae [Fig. 6, case (ii)]. The growth of tricalcium phosphate and tetracalcium phosphate may delay the growth of oxyapatite with the latent heat of fusion. With a high level of dehydroxylation in the molten particle, less hydroxyapatite, and hence, less oxyapatite, will form, and so the large volume of dehydroxylated material will then mostly contain tricalcium phosphate and tetracalcium phosphate. The growth mechanism may begin within the droplet, since a more fluid droplet facilitates faster diffusion.

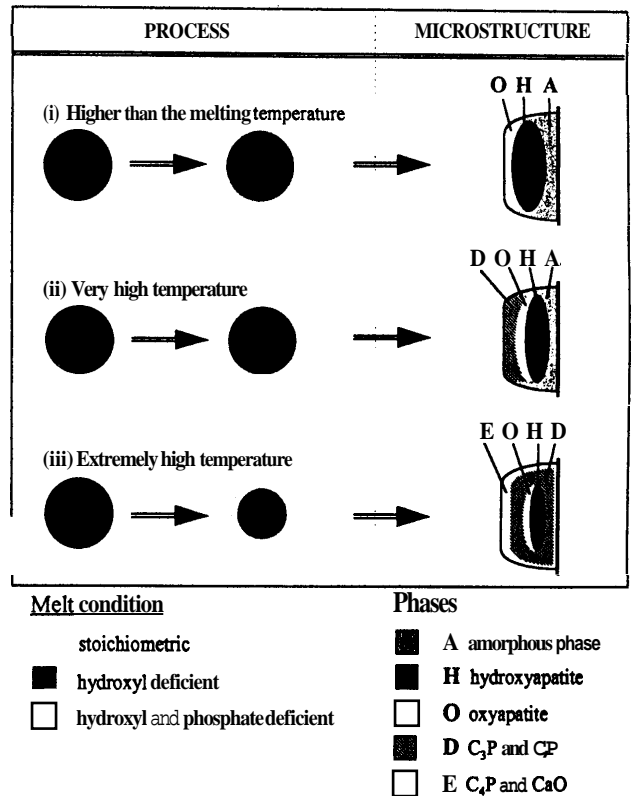


Figure 6. A proposed model for phase formation in plasma-sprayed hydroxyapatite coatings. The process stage depicts the various melt chemistries as a function of particle temperature. The microstructure depicts the different phases that can be formed in a lamellae.

Calcium oxide is observed when higher heating conditions are employed. In addition to being hydroxyl deficient, the outer shell of the molten particle also becomes phosphate deficient [Fig. 6, case (iii) (process stage)]. Loss of one  $P_2O_5$  from the unit cell shifts the composition from 56.8 wt % CaO for hydroxyapatite to 66.4 wt %, which consists of a two-phase field containing calcium oxide and tetracalcium phosphate [Fig. 1(b)]. Given a significant  $P_2O_5$  loss, calcium oxide will readily crystallize together with tetracalcium phosphate. Calcium oxide is very reactive with water and is not desired in hydroxyapatite coatings for implants or prostheses.

The situation of distinct chemical regions of a fixed thickness within the droplet and uniformly thick lamellae, as shown in the model, rarely occurs in practice. Particles will experience nonuniform heat transfer during flight and may be partially or totally molten. For example, angular particles will experience higher dehydroxylation and more phosphate removal from more heat transfer. Droplets with a depleted phosphate content can then deposit and may form an amorphous phase.<sup>30</sup>

The molten particle is subjected to splashing on the substrate, leading to satellite droplets which consist of phases dictated by the composition and cooling conditions. Furthermore, a molten particle will experience relative motion with the underlying surface produced by rough surfaces or substrates positioned at angles other than the perpendicular to the spray stream. The relative motion will displace these compositional regions and could lead to flow of the more fluid hydroxylated liquid<sup>31</sup> from the core onto the substrate. These areas will consequently produce the amorphous phase in place of tricalcium phosphate and tetracalcium phosphate, as indicated in Figure 6, case (iii). Similarly, the other compositional regions may be displaced depending upon the forces at impact with the substrate and the viscosity of the liquids.

Figure 7 shows the amorphous areas as regions of darker appearance more predominant at the substrate. The lighter areas correspond to the crystalline phase. Few techniques are available to examine the location of the different phases within the microstructure. Transmission electron microscopy offers one possibility, but the examination of oxyapatite is not possible owing to dehydroxylation.<sup>32</sup>

Standards for hydroxyapatite coatings restrict the phases within coatings and correspond to conditions of low heat transfer. A concentration of 5 wt %  $C_3P$  is permitted with a high crystalline phase content within the coating. This combination of phases can be obtained with a large particle-sized powder sprayed at low heat inputs. The starting powder should be stoichiometric hydroxyapatite, and therefore not be heat treated in a vacuum furnace. By providing a more uniform phase composition in the coating, the coating



**Figure 7.** A polished cross section of a hydroxyapatite coating exhibiting the amorphous phase (dark gray) and crystalline phases (light gray). The white area to the far left represents the substrate. The magnification bar is 50  $\mu\text{m}$  wide.

degradation will be minimized and bone tissue will be able to biointegrate with a hydroxyapatite coating.

## CONCLUSIONS

The functionality of plasma-sprayed hydroxyapatite depends on the structure and the chemical composition of phases within the coating. Thus, since the present work indicates that the phases can be altered by the processing conditions, there is the ability to control the *in vitro* response of these implants.

The authors are grateful for the X-ray fluorescence studies conducted by Dr. H. Wang of Sherritt Gordon, Inc.

## References

1. A. McNab, "Hydroxyapatite orbital implants," *Aust. NZ J. Ophthalmol.*, **23**, 117–123 (1995).
2. H. Aoki, M. Akao, Y. Shin, Y. Tsuzi, and T. Togawa, "Sintered hydroxyapatite for a percutaneous device and its clinical applications," *Med. Progr. Technol.*, **12**, 213–220 (1987).
3. R. J. Cronin, L. J. Oesterle, and D. M. Ranly, "Mandibular implants and the growing patient," *Int. J. Oral Maxillofac. Implants*, **9**, 55–62 (1994).
4. O. R. Beirne, T. A. Curtis, and J. S. Greenspan, "Mandibular augmentation with hydroxyapatite," *J. Prosthet. Dent.*, **55**, 362–366 (1985).
5. K. Soballe and S. Overgaard, "The current status of hydroxyapatite coating of prostheses (editorial)," *J. Bone Joint Surg.*, **78B**, 689–691 (1996).
6. M. Zablotsky, "HA coatings in implant dentistry: Hype, hysteria, or clinical reality?" *J. Dent. Symp.*, **1**, 70–72 (1993).
7. C. M. Cottel, D. B. Chrisey, K. S. Grabowski, J. A. Sprague, and C. R. Gossett, "Pulsed laser deposition of hydroxyapatite thin films on Ti-6Al-4V," *J. Appl. Biomater.*, **3**, 87–93 (1992).

8. J. A. Jansen, J. G. C. Wolke, S. Swann, J. C. P. M. van der Waerden, and K. de Groot, "Application of magnetron sputtering for producing ceramic coatings on implant materials," *Clin. Oral Implants Res.*, **4**, 28–34 (1993).
9. J. D. deBruijn, Y. P. Bovell, and C. A. van Blitterwijk, "Structural arrangements at the interface between plasma sprayed calcium phosphates and bone," *Biomaterials*, **15**, 543–550 (1994).
10. P. Ducheyne, S. Radin, and L. King, "The effect of calcium phosphate ceramic composition and structure on in vitro behavior: I. Dissolution," *J. Biomed. Mater. Res.*, **27**, 25–34 (1993).
11. P. V. Riboud, "Composition and stability of apatites in the system  $\text{CaO-P}_2\text{O}_5\text{-iron oxide-H}_2\text{O}$  at high temperature," *Ann. Chim.*, **8**, 381–390 (1973).
12. R. W. Nurse, J. H. Welch, and W. Gutt, "A new form of tricalcium phosphate," *Nature*, **182**, 1230 (1958).
13. L. Ruan, X. Wang, and L. Li, "Structural analysis of new crystal phase for calcium phosphate in  $\alpha_1 \leftrightarrow \alpha'$  phase transition," *Mat. Res. Bull.*, **31**, 1207–1212 (1996).
14. K. Lohberg and H. Muller, "Unterkuhlarbeit extrem rasch abgekühlter Schmelzen von Kupfer und Kupfermischkristallen und deren Gefügeausbildung," *Z. Metallkd.*, **60**, 231–237 (1969).
15. K. A. Gross, C. C. Berndt, and H. Herman, "Amorphous phase formation in plasma-sprayed hydroxyapatite coatings," *J. Biomed. Mater. Res.*, **39**, 407–414 (1998).
16. K. A. Gross, V. Gross, and C. C. Berndt, "Thermal analysis of the amorphous phase in hydroxyapatite coatings," *J. Am. Ceram. Soc.*, in press.
17. ASTM 1185-88, Standard specification for composition of ceramic hydroxylapatite for surgical implants, 1988.
18. M. Vardelle, A. Vardelle, P. Fauchais, C. Trassy, and P. Proulx, "Experimental and numerical investigation of powder vaporization under thermal plasma conditions," *Colloque de Physique, Colloque C5, Suppl.* **18**, 171–180 (1990).
19. K. G. Shaw, M. F. Gruninger, and W. J. Jarosinski, "High temperature intermetallic binders for HVOF carbides," in *Thermal Spray Industrial Applications*, C. C. Berndt and S. Sampath (eds.), ASM International, Materials Park, Ohio, 1994, pp. 185–190.
20. G. Chambon, C. Trassy, M. Vardelle, A. Vardelle, and P. Fauchais, "Investigations of WC-Co particles vaporization in a thermal plasma jet," *J. High Temp. Chem. Process.*, **1**, 231–239 (1992).
21. R. Neiser, "Structure–processing–property relationships in air plasma sprayed  $\text{YBa}_2\text{Cu}_3\text{O}_{7-x}$ ," PhD thesis, SUNY Stony Brook, 1989.
22. J. H. Welch and W. Gutt, "High temperatures studies of the system calcium oxide-phosphorus pentoxide," *J. Chem. Soc.*, **IV**, 4442–4444 (1961).
23. K. Yamashita, T. Arashi, K. Kitagaki, S. Yamada, T. Umegaki, and K. Ogawa, "Preparation of apatite thin films through rf-sputtering from calcium phosphate glasses," *J. Am. Ceram. Soc.*, **77**, 2401–2407 (1994).
24. B. C. Wang, E. Chang, C. Y. Yang, D. Tu, and C. H. Tsai, "Characteristics and osteoconductivity of three different plasma-sprayed hydroxyapatite coatings," *Surf. Coat. Technol.*, **58**, 107–117 (1993).
25. R. McPherson, N. Gane, and T. J. Bastow, "Structural characterization of plasma-sprayed hydroxylapatite coatings," *J. Mater. Sci. Mater. Med.*, **6**, 327–334 (1995).
26. L. G. Ellies, D. G. A. Nelson, and J. D. B. Featherstone, "Crystallographic changes in calcium phosphates during plasma-spraying," *Biomaterials*, **13**, 313–316 (1992).
27. C. Y. Yang, B. C. Wang, E. Chang, and J. D. Wu, "The influences of plasma spraying parameters on the characteristics of hydroxyapatite coatings: A quantitative study," *J. Mater. Sci. Mater. Med.*, **6**, 249–257 (1995).
28. M. Knepper, "Entwicklung plasmagespritzter calcium-phosphat-schichten für den Einsatz in der Medizintechnik," PhD dissertation, Technical University of Aachen, 1993.
29. K. A. Khor and P. Cheang, "Characterization of plasma sprayed hydroxyapatite powders and coatings," in *Thermal Spray Coatings: Research, Design and Applications*, C. C. Berndt and T. F. Bernecki (eds.), ASM International, Materials Park, Ohio, 1993, pp. 347–352.
30. J. Vogel, C. Russel, G. Gunther, P. Hartman, F. Vizethium, and N. Bergner, "Characterization of plasma-sprayed hydroxyapatite by  $^{31}\text{P}$ -MAS-NMR and the effect of subsequent annealing," *J. Mater. Sci. Mater. Med.*, **7**, 495–499 (1996).
31. O. N. Kanchieva, N. V. Komarova, S. V. Nemilov, and D. K. Tagantsev, "Effect of water content on the viscosity of glassy sodium oxide-2-(silicon dioxide) ( $\text{Na}_2\text{O} \cdot 2\text{SiO}_2$ ), lead oxide-2-(boron oxide) ( $\text{PbO} \cdot 2\text{B}_2\text{O}_3$ ), and calcium oxide-phosphorus pentoxide," *Fiz. Khim. Stekla*, **6**, 408–414 (1980).
32. H. Ji and P. M. Marquis, "Modification of hydroxyapatite during transmission electron microscopy," *J. Mater. Sci. Lett.*, **10**, 132–134 (1991).